

Synthetic tambjamine analogues induce mitochondrial swelling and lysosomal dysfunction leading to autophagy blockade and cell death in lung cancer

Ananda M. Rodilla¹, Luís Korrodi-Gregório^{1,2}, Elsa Hernando³, Pilar Manuel-Manresa¹, Roberto Quesada³, Ricardo Pérez-Tomás^{1*} and Vanessa Soto-Cerrato^{1*}.

¹Cancer Cell Biology Research Group, Department of Pathology and Experimental Therapeutics, Faculty of Medicine, University of Barcelona, Barcelona, Spain

² Laboratory of Signal Transduction, Department of Medical Sciences, Institute for Research in Biomedicine - iBiMED, Health Sciences Program, University of Aveiro, Aveiro, Portugal.

³ Department of Chemistry, University of Burgos, Burgos, Spain

* Corresponding authors: Dr. Vanessa Soto-Cerrato, e-mail: vsoto@ub.edu, Tel. +34934031140, Fax. +34 934024249; Dr. Ricardo Pérez-Tomás, e-mail: rperez@ub.edu, Tel/Fax. +34 934024288. Cancer Cell Biology Research Group, Department of Pathology and Experimental Therapeutics, Faculty of Medicine, University of Barcelona, C/Feixa Llarga s/n, 08907 L'Hospitalet de Llobregat, Barcelona, Spain.

E-mail addresses: ananda.rodilla@ub.edu (A.M.R.); korrodi@ub.edu (L.K.G.); ehsanta@ubu.es (E.H.); pilarmanuel@ub.edu (P.M.M.); rquesada@ubu.es (R.Q).

ABSTRACT

Current pharmacological treatments for lung cancer show very poor clinical outcomes, therefore, the development of novel anticancer agents with different mechanisms of action is urgently needed. Cancer cells have a reversed pH gradient compared to normal cells, which favors cancer progression by promoting proliferation, metabolic adaptation and evasion of apoptosis. In this regard, the use of ionophores to modulate intracellular pH appears as a promising new therapeutic strategy. Indeed, there is a growing body of evidence supporting ionophores as a novel antitumor drugs. Despite this, little is known about the implications of pH deregulation and homeostasis imbalance triggered by ionophores at the cellular level. In this work, we deeply analyze for the first time the anticancer effects of tambjamine analogues, a group of highly effective anion selective ionophores, at the cellular and molecular level. First, their effects on cell viability were determined in several lung cancer cell lines and patient-derived cancer stem cells, demonstrating their potent cytotoxic effects. Then, we have characterized the induced lysosomal deacidification, as well as, the massive cytoplasmic vacuolization observed after treatment with these compounds, which is consistent with mitochondrial swelling. Finally, the activation of several proteins involved in stress response, autophagy and apoptosis was also detected, although necrosis was the main mechanism of cell death induced.

Altogether, these evidences suggest that tambjamine analogues provoke an imbalance in cellular ion homeostasis that triggers mitochondrial dysfunction and lysosomal deacidification leading to a potent cytotoxic effect through necrosis in lung cancer cell lines and cancer stem cells.

Keywords

Anionophores, synthetic tambjamine analogues, intracellular pH, lysosomal dysfunction, autophagy.

1. Introduction

Correct ion exchange through cellular membranes is an essential process for maintaining osmotic balance and intracellular pH (pHi) [1], which are key parameters controlling many biological processes. In fact, variations in cellular concentrations of certain ions coordinate the signals that converge on cell cycle checkpoints [2], regulating the proliferative capacity of cells and their differentiation. Similarly, the triggering of the apoptotic programmed cell death also depends on ion fluxes mediated by cellular ion channels [3]. Therefore, when cellular pH is not preserved at a favourable level, different pathologies may appear, as it is the case of cancer. Cancer cells undergo a pH deregulation during the process of carcinogenesis, resulting in the acidification of the extracellular pH (pHe) and the alkalinisation of the pHi. This adaptive reversed pH gradient is decisive for survival and propagation of tumours, promotes metabolic adaptation, evasion of apoptosis and facilitates the metastatic dissemination of tumour cells. Consequently, pH is recently being considered as another hallmark of cancer [4].

Among different cancers, lung cancer remains a major public health problem since it is the leading cause of mortality related to this disease, accounting for more than 1.5 million deaths in 2012 [5]. Early diagnosis and advances in first-line treatments are not entirely effective in reducing this high mortality since conventional treatments have limited success. Therefore, the identification of novel anticancer compounds focused on different mechanisms of action is eagerly needed [6, 7].

Based on the specific altered pH of cancer cells, modulation of intracellular pH has recently been proposed as a new therapeutic strategy against cancer. In this regard, a diverse group of anionophores, lipid soluble compounds that facilitate the transport of anions across cell membranes, have recently emerged as promising anticancer compounds [8, 9]. Indeed, prodigiosin, a tripyrrolic natural product with anticancer properties, represents one of the first described anionophores [10-13]. It has been reported that its biological activity is partly due to its ability to deacidify acidic compartments within cells, which may cause a drop in pHi, and therefore the onset of apoptosis in cancer cells [9, 11, 14]. Emulating that characteristic, different anionophores have been designed and evaluated [15]. We focused our attention on the bioactive marine alkaloids tambjamines, other class of natural

anionophores which have shown interesting cytotoxic [16, 17]. We have recently synthesized novel synthetic tambjamine analogues bearing aromatic substituents in the enamine moiety, as well as explored different substitution patterns on characteristic alkoxy group of the central pyrrole ring. These compounds proved to be very efficient anion exchangers in liposome models, promoting both chloride and bicarbonate transport [18-20]. As a result of this anionophoric activity, compounds bearing 4-alkoxy-2,2'-bipyrrole moieties have shown to possess interesting anticancer activities in a wide panel of cancer cell lines [19]. Moreover, a different type of tambjamine analogues, in which the characteristic 2,2'-bipyrrole unit is replaced by a 2-pyrrolylindole, have recently shown the ability to hyperpolarize the cellular membrane as well as differentiate and induce cell death in lung cancer stem cells [20], which are promising properties for their potential use in cancer therapy.

Despite the identification of this class of anion selective ionophores as novel potential anticancer drugs, very little is known about the effects at the cellular level of the facilitated anion transport and the implications of unbalanced homeostasis and pH deregulation in the cytotoxicity exhibited by anionophores. In the present work, we analyse in detail for the first time the cellular and molecular mechanisms of action that lead to the cell death triggered by these potent anionophores in several lung cancer cell lines and cancer stem cells (CSC).

2. Materials and Methods

2.1. Compounds synthesis

Tambjamine analogues (Figure 1a) were synthesized as previously reported [19]. Drugs were dissolved at 10 mM in DMSO and stored at -20°C. Subsequent dilutions for biological assays were made in culture medium.

2.2. Cell lines and culture conditions

Human lung cancer cell lines A549 (adenocarcinoma), DMS53 (small cell carcinoma), H460 (large cell carcinoma) and SW900 (squamous carcinoma) were obtained from the American Type Culture Collection (ATCC, Manassas VA), and maintained in DMEM (A549) or RPMI media (Biological Industries, Beit Haemek, Israel). All media were supplemented with 100 U/mL penicillin, 100 µg/mL streptomycin, and 2 mM L-glutamine, all from Biological

Industries and 10% foetal bovine serum (FBS; Gibco, NY, USA). Cancer stem cells were obtained from resected patient tumour samples or isolated from cancer cell lines and characterized through evaluation of stem cell surface markers (CD166, CD44, CD90, CD133 and EpCAM) by flow cytometry. Moreover, tumorigenic properties of tumour spheres were assessed through subcutaneous transplantation in NOD.CB17-Prkdc^{scid}/NcrCrI mice (Jackson Laboratories) and tumor growth curves were monitored. For detailed procedures and results see supplementary information in reference [20]. CSC were cultured as a cell suspension in RPMI media supplemented with 50 µg/mL EGF, 20 µg/mL bFGF, 1X ITS, 0.4% BSA and 2% B27 (Gibco, Paisley, UK). Cells at passage 10-25 were grown at 37°C under a 5% CO₂ atmosphere.

2.3. Cell viability assay

Cell viability was determined by the MTT assay [21]. Cells (1×10^5 cells/mL) were seeded in 96-well microtiter plates and incubated for 24 h to allow cells to attach. Afterwards, they were treated for 24 h with 10 µM of each compound for single point experiments and dose-response curves were performed ranging from 0.78 to 100 µM to calculate the inhibitory concentrations of 25%, 50% and 75% of cell population (IC₂₅, IC₅₀, and IC₇₅ values). Cisplatin and DMSO were used as positive and negative controls, respectively. In the case of positive control, concentrations ranging from 1.56 to 200 µM were tested. For inhibition assays, the apoptotic inhibitor Z-VAD-FMK (10 µM) or the autophagic inhibitor 3-MA (5 mM) were added 30 min prior compound **2** addition. After 24 h, 10 µM of 3-(4,5-dimethylthiazol-2-yl)-2,5-diphenyltetrazolium bromide diluted in 1X PBS (MTT, Sigma-Aldrich) was added to each well for an additional 4 h. The medium was removed and the MTT formazan precipitate was dissolved in 100 µL of DMSO. Absorbance was read on a Multiskan multiwell plate reader (Thermo Fisher Scientific Inc., Waltham, MA, USA) at 570 nm. For each condition, at least three independent experiments were performed in triplicate. Cell viability was expressed as a percentage of control cells, and data are shown as the mean value ± S.D. The IC₂₅, IC₅₀ and IC₇₅ values were calculated with GraphPad Prism 5 software.

For single-point cell viability assays in monolayer cells (passage 10-20) and spheres-forming cells (passage 1-2), they were plated at the desired density ($1-2 \times 10^3$ or $2-3.5 \times 10^3$, respectively) in 200 µL per well in 96-well plates. One day (24 h) after seeding, compound **2** was added in three replicates at 10 µM for each cell line or patient's derived cultures.

Patient samples acquisition protocol and informed consent were approved by the local ethics committee. Cell viability was measured after 24 h, using the CellTiter 96® AQueous One Solution Cell Proliferation Assay (Promega, Madison, WI, USA) and following the manufacturer's instructions. Absorbance at 490 nm was detected using a VICTOR3 Multilabel Plate Reader (Perkin Elmer-Cetus, Norwalk, CT). Cell viability was normalized to the respective control cells and presented as a percentage of them. For each condition, three independent experiments were performed and mean \pm SD is shown.

2.4. ISE transport assays

A chloroform solution (20 mg/mL) of 1-palmitoyl-2-oleoyl-sn-glycero-3-phosphocholine (POPC) (Sigma-Aldrich, St Louis, MO, USA) was evaporated *in vacuo* using a rotary evaporator and the resulting lipid film was dried under vacuum for at least 2 h. After that, it was rehydrated by addition of a sodium chloride solution (489 mM NaCl and 5 mM phosphate buffer, pH 7.2 or 451 mM NaCl and 20 mM phosphate buffer, pH 7.2) followed by careful vortexing. The obtained lipid suspension was subjected to nine freeze-thaw cycles and twenty-nine extrusions through a 200 nm polycarbonate Nucleopore membrane using a LiposoFastBasic extruder (Avestin Inc., Ottawa, Canada). In order to remove the unencapsulated chloride, the obtained vesicles were dialyzed against a NaNO₃ solution (489 mM NaNO₃ and 5 mM phosphate buffer, pH 7.2) or a Na₂SO₄ solution (150 mM Na₂SO₄ and 20 mM phosphate buffer, pH 7.2), respectively. For the NO₃⁻/Cl⁻ assays, vesicles prepared as described above (rehydrated with 489 mM NaCl), were suspended in a solution 489 mM NaNO₃ and 5 mM phosphate buffer, pH 7.2 to a final lipid concentration of 0.5 mM in a total volume of 5 mL. Using a chloride selective electrode (CRISON 96 52 C I.S.E. electrode) the chloride efflux was monitored over time. After 60 s, an aliquot of the transmembrane anion carrier in DMSO was added (the amount of DMSO was always less than 20 μ L in order to avoid influence of the solvent molecules in the assay). After five minutes (t=360 s), a pulse of detergent was added (Triton X-100 10% dispersion in water, 20 μ L), thus vesicles were lysed. The obtained final reading was considered as the 100% of the chloride encapsulated and used as such. For (HCO₃⁻/Cl⁻) assays, the vesicles were rehydrated with 451 mM NaCl and suspended in the Na₂SO₄ solution. Again, the final lipid concentration in each experiment was 0.5 mM and the total volume in each experiment 5 mL. A volume of the carrier molecule was added at the beginning of the experiment (t=0 s). A minute later (t=60 s), an aliquot of

NaHCO₃ (in 150 mM Na₂SO₄ buffered to pH 7.2 with 20 mM sodium phosphate salts) was added for a final concentration of 40 mM. The chloride efflux was measured during 5 min and then the detergent was added (t=360 s). The data were used as described previously.

2.5. Acridine Orange staining

A549 cells (1 × 10⁵ cells/well) grown in a 12-well plate with cover slips for 24 h were treated with or without the IC₅₀ value of the studied compounds for 1 h (DMSO was added in control cells). Afterwards, cells were washed twice with 1X PBS and stained with 5 µg/mL acridine orange (AO) solution for 30 min at room temperature. Finally, they were washed three times with 1X PBS/10% FBS and fluorescence was immediately examined in a NIKON eclipse E800 microscope (filter 330/380 nm). Three independent experiments were conducted and representative images are shown.

2.6. Phase contrast microscopy

For cytoplasmic vacuolization observation, A549 cells (1 × 10⁵ cells/mL) were seeded in a 6-well plate and allowed to grow for 24 h, subsequently cells were treated with the IC₇₅ values of each compound during 6 h and images were observed under inverted phase contrast microscope (Axio Observer Z1). For cell monitoring, A549 cells (1 × 10⁵ cells/mL) were seeded in 96-well microtiter plates and incubated for 24 h to allow cells to attach. Afterwards, they were treated for 24 h with 10 µM of each compound. Then, images were captured following a time course from 0 (before adding drug) to 24 h with a Leica inverted phase-contrast microscope DMIRBE equipped with digital capture software (Leica Microsystems, Wetzlar, Germany).

2.7. Immunofluorescence microscopy

A549 cells (2 × 10⁵ cells/mL) were cultured in a 12-well plate containing glass coverslips and were incubated with the IC₇₅ of the studied compounds for 6 h. Cells were then washed twice with 1X PBS and fixed with 4% paraformaldehyde for 20 min. Fixed cells were permeabilized with 0.2% Triton X-100 and then blocked with 1% BSA in 1X PBS for 1 h. Cells were incubated overnight at 4°C with anti-LC3 (1:500 dilution, Cat#PM036) from MBL International Corporation or anti-TOMM20 (1:200 dilution, Cat#612278) from BD Biosciences (San Jose, CA, USA). In case of using anti-EEA1 (1:1000 dilution, Cat#ab2900) and

anti-LAMP1 (1:1000 dilution, Cat#ab24170) both from Abcam (Cambridge, MA, USA) cells were permeabilized with 0.2% Saponin, for 15 min, and then blocked with 0.2% gelatin-20% normal goat serum in 1X PBS for 1 h at room temperature.

Cells were then washed with 1X PBS and incubated with Alexa Fluor 555-conjugated donkey anti-mouse (Cat#A31570, Molecular Probes, Eugene, OR, USA) or Alexa Fluor 555-conjugated donkey anti-rabbit (Cat#A31572, Molecular Probes) at 1:400 dilution for 1 h at room temperature. At the same time, the nuclear marker TOPRO-3 iodide (1:400, Cat#T3605, Molecular Probes) was added. Afterwards, coverslips were washed with 1X PBS and were placed on the slides using mowiol (Sigma-Aldrich). The immunofluorescence images were captured using a Leica TCS-SL filter-free spectral confocal microscope (Leica Microsystems). Representative images from three independent experiments are shown.

2.8. mCherry-Mito7 stable transfection in A549 cells

A549 cells (3×10^5 cells/mL) were seeded in 60 mm plates and allowed to grow up to 80% confluence. Before transfection, growth media was replaced by Optimem media without FBS (Gibco) and 8 μg of plasmid DNA (mCherry-Mito-7 was a gift from Michael Davidson (Addgene plasmid # 55102) [22] was transfected using 20 μL of lipofectamine reagent (Invitrogen, Carlsbad, CA, USA) per condition. After 5 h of transfection, the media was replaced by complete media. Stable selection was performed by adding G418 (Calbiochem, La Jolla, CA) to the media at 800 $\mu\text{g}/\text{mL}$ final concentration 2 days after the transfection. After 3 weeks, the brightest cell population was selected by cell sorting using a Moflo Astrios XPD Cell Sorter (Beckman Coulter, Miami, FL, USA). When a stable mCherry-Mito7 overexpressing A549 cell line was established, cells were seeded in a μ -Slide chambered coverslip (Ibidi), and allowed them to attach and grow during 72 h. Afterwards, cells were exposed to IC_{75} of the studied compounds and a far-red nuclear counterstain, DRAQ5 (Abcam) was applied at a 1:5,000 dilution. The images were captured every 20 min for 3 h using a Leica TCS-SL filter-free spectral confocal microscope (Leica Microsystems). Representative images from three independent experiments are shown.

2.9. Transmission electron microscopy

A549 cells (2×10^5 cells/mL) grown in 100 mm plates and were incubated with the IC_{75} of the studied compounds for 6 h. Cells were fixed in a solution containing 2% paraformaldehyde, 2.5% glutaraldehyde in 0.1 M phosphate buffer (pH 7.2) at room temperature for 1 h and then collected as cell pellets. Pellets were kept in a post-fixed solution containing 1% osmium tetroxide, 0.8% potassium ferrocyanide in 0.1M phosphate buffer (pH 7.2) at 4°C. After that, cells were dehydrated in graded acetone, embedded in Spurr's resin and cured at 60°C for 48 h. Semithin sections (1 μ m) were cut with a glass knife, mounted on slides, stained with 1% methylene blue and viewed using a light microscope to select the region of interest. Ultrathin sections (60-70 nm) were cut using a diamond knife, mounted on 200 mesh copper grids and double-stained with 2% aqueous uranyl acetate (for 30 min) and Reynold's lead citrate (for 10 min). Specimens were examined in a transmission electron microscope Jeol 1010 (Jeol, Tokyo, Japan) and digital images were acquired using a Gatan Orius SC1000 CCD Digital Camera. Two independent experiments were performed and photographs were taken from at least three different semithin sections from each experiment.

2.10. Mitotracker staining

A549 cells (1×10^4 cells/well) were seeded in 8-well sterile μ -Slide (chambered coverslip) (Ibidi, Martinsried, Germany), and allowed to attach and grow during 72 h. Then, cells were preincubated with MitoTracker Red CMXRos 500 nM during 1 h, washed with 1X PBS and exposed to IC_{75} value of compound **2** for 3 h. Immunofluorescence images were captured using a Leica TCS-SL filter-free spectral confocal microscope (Leica Microsystems). Representative images from three independent experiments are shown.

2.11. Immunoblot analysis

A549 cells (1×10^5 cells/mL) were seeded and allowed to grow for 24 h. Afterwards, they were exposed to compounds (IC_{25} , IC_{50} and IC_{75} values) for 24 or 48 h. Total protein extracts were obtained from cells by the addition of lysis buffer (0.1% SDS, 1% NP-40, 0.5 % sodium deoxycholate, 50 mM NaF, 40 mM β -glycerophosphate, 200 μ M sodium orthovanadate, 1 mM phenylmethylsulfonyl fluoride, serine and cysteine protease inhibitor cocktail (Roche Mannheim, Germany) in 1X PBS). Protein concentration was determined by BCA protein assay (Pierce, Rockford, IL, USA) using bovine serum albumin (BSA) as a standard. After that,

40 µg of protein extracts were separated by 8-15% SDS-polyacrylamide gel electrophoresis and transferred to Immobilon-P membranes (Millipore, Bedford, MA, USA). Membranes were blocked in 5% dry milk or 5% BSA, both diluted in 1X TBS–Tween (50 mM Tris–HCl pH 7.5, 150 mM NaCl, 0.1% Tween 20) for 1 h and then incubated overnight with primary antibodies, according to the manufacturer’s instructions. Antibodies were obtained from the following sources: anti-caspase 3 (Cat#9662), anti-caspase 9 (Cat#9502), anti-PARP (Cat#9542), anti-phospho-p38 MAPK (Thr180/Tyr182, Cat#4511), anti-p38 MAPK (Cat#8690), from Cell Signaling Technology (Beverly, MA, USA); anti-LC3 (Cat#PM036) and anti-p62/SQSTM1 (Cat#PM045) both from MBL International Corporation (Woburn, MA, USA); anti-actin (I-19, Cat#sc-1616) from Santa Cruz Biotechnology (Santa Cruz, CA) and anti-vinculin (Cat#V-4505) from Sigma-Aldrich. Antibody binding was detected with goat anti-mouse IgG-HRP (Cat#sc-2005), goat anti-rabbit IgG-HRP (Cat#sc-2004) and donkey anti-goat IgG-HRP (Cat#sc-2020) all from Santa Cruz Biotechnology, and the ECL detection kit (Amersham, Buckinghamshire, UK). Actin or vinculin were used as gel loading controls. Results shown are representative of Western blot data obtained from at least three independent experiments with similar observations. Images were captured on an Image Quant LAS 500 (GE Healthcare Little Chalfont, UK) and band densitometries were retrieved using the software ImageJ version 1.43u software (National Institutes of Health, Bethesda, Maryland, USA).

2.12. Statistical analyses

Results are expressed as the mean ± SEM of at least three independent experiments. One-way ANOVA analyses were carried out with the Statgraphics centurion statistical package and post-hoc Tukey analyses were performed. Statistically significant differences, $p < 0.05$ and $p < 0.01$, are represented by * and **, respectively.

3. Results

3.1. Compounds cytotoxic effects on cancer cell lines and cancer stem cells

The effect on cell viability of several tambjamine analogues (Figure 1a), selected from a previous screening [19], was evaluated in different lung cancer cell lines representative of

the four major histological subtypes (A549, adenocarcinoma; SW900, squamous cell carcinoma; H460, large cell carcinoma; DMS53, small-cell carcinoma) (Figure 1b). Cell viability was measured by the MTT assay and a significant decrease (more than 50%) was observed after 24 h with 10 μM of all the tested compounds. From these experiments two derivatives (compounds **2** and **7**) were selected as the most potent compounds. Then, dose-response experiments were conducted in A549 cells and compared to a positive control, cisplatin as a current chemotherapeutic treatment in lung cancer. The IC_{50} values obtained for compound **2** and **7** were 3.38 ± 0.98 and 1.67 ± 0.29 μM and IC_{75} values were 4.72 ± 0.76 and 3.57 ± 0.49 μM , respectively; while IC_{50} value for cisplatin (CDDP) was more than 200 μM (Figure 1c).

Cell viability after treatment with the most potent compound, tambjamine **2**, was also evaluated in cancer stem cells (CSC) derived from patients or isolated from cancer cell lines (Figure 1d). The derived tumour spheres were deeply characterized, showing enrichment in stem cell surface markers as well as great tumorigenic properties in scid mice transplantation experiments (see supplementary information reference [20]). Our results show a significant decrease in cell viability, either in CSC derived from cell lines (A549 and SW900) or derived from tumour patient samples (FIS302 and FIS303).

3.2. Tambjamine derivatives are effective anion transporters

The activity as transmembrane anion carriers of the two most cytotoxic compounds, **2** and **7**, was assayed in model POPC liposomes. Chloride loaded liposomes were suspended in an isotonic chloride free medium, and chloride efflux facilitated by these compounds was monitored using a chloride selective electrode. At the end of the experiments, vesicles were lysed by the addition of detergent and the final electrode reading considered as 100% chloride release. Quantification of the transport activity was carried out by repeating the experiments using several concentrations of the studied compounds and performing hill analyses of the results (Figure 2a and b). The resulting EC_{50} value represents the amount of compound needed to release 50% of the encapsulated chloride in the time scale of the experiments (300 s). The EC_{50} values obtained for **2** and **7** were 50 nM and 60 nM respectively in the assay involving NaNO_3 as external solution and 240 nM and 880 nM respectively in the assay involving NaHCO_3 as external solution. The impact on the EC_{50}

values of the external anion is consistent with an exchange mechanism in which chloride efflux from the interior of the vesicle is accompanied by influx of the external anion, thus precluding the formation of an electrochemical gradient. The relative higher lipophilicity of nitrate compared to bicarbonate makes this later anion more difficult to extract into the membrane hydrophobic core and hence the higher EC₅₀ observed. This transport mechanism has been studied by us in detail and the result demonstrate that **2** and **7** are very potent anionophores promoting effective transmembrane anion transport in vesicles at low loadings [19].

3.3. Lysosomal pH deregulation

Lysosomal pH modifications in A549 cells were analysed using acridine orange staining [23]. This dye accumulates into acidic organelles, like lysosomes or late endosomes, and emits orange fluorescence as a result of its protonation under these acidic pH conditions, whilst it emits green fluorescence in other parts of the cell, as observed in control cells (Figure 2c). When A549 cells were treated with IC₅₀ values of compounds **2** or **7** for 1 h, the orange fluorescence in the vesicle compartments disappeared, indicating an increase in the pH of these organelles. This result is in agreement with the ionophoric activity of these compounds facilitating the transmembrane transport of anions such as bicarbonate across cellular membranes and this pH alteration should result in lysosomal dysfunction.

3.4. Cytoplasmic vacuolization induced by tambjamine analogues

After treatment with compounds **2** or **7**, massive cytoplasmic vacuolization was observed by phase contrast microscopy after 6 h exposure with their IC₇₅ values (Figure 3a). To better understand this phenomenon, cells were monitored during 24 h after 10 μM treatment with each compound (Figure 3b). Cytoplasmic vacuolization was observed as soon as 3 h of compounds addition and was maintained up to 24 h. In the case of compound **2**, cell death due to cellular swelling and/or burst was observed within the 24 h period. This is indicative of necrotic cell death reflecting the potent cytotoxic activity of this compound.

In order to determine which cellular organelle was undergoing this vacuolization process, several subcellular markers were used for immunofluorescence detection (Figures 4 and 5). First of all, the autophagosomal marker LC3 was evaluated and, although a high increase on

protein levels was observed, it did not colocalize with the vacuoles (Figure 4a). Then, the lysosomal marker LAMP1 and the early endosomal marker EEA1 were used and different protein localization was observed in treated cells, but again neither colocalized with the vacuolated organelle (Figure 4b and 4c). Moreover, the hydrophilic polysaccharide dextran-red was administered to treated cells to monitor macro/pinocytosis, but we did not obtain vesicle staining (data not shown). Finally, a mitochondrial protein called TOMM20 was employed and proved to stain the membranes of the vacuoles, indicating that mitochondrial swelling was occurring after compound treatment (Figure 5a) and ruling out vacuolization of autophagosomes, lysosomes or endosomes.

3.5. Mitochondrial swelling

To further characterize that the vacuolated organelle was mitochondria, a plasmid with the mitochondrial targeting sequence from subunit VIII of human cytochrome c oxidase was transfected into cells in order to monitor mitochondria. Control cells showed typical red mitochondrial staining, whereas in cells treated with compound **2**, mitochondrial swelling was clearly observed (Figure 5b). Transmission electron micrographs were obtained from control and cells treated with compounds **2** or **7** to analyse these results in deep, and mitochondrial swelling was also observed (black arrows, Figure 5c). Moreover, many autophagy-related structures such as autophagosomes, autolysosomes and dense lysosomes are also visualized in treated cells.

This process was also studied using MitoTracker Red CMXRos, a fluorescent dye whose accumulation depends on mitochondrial membrane potential [24], to track mitochondria (Figure 6). Control cells showed typical filamentous mitochondria, but in treated cells mitochondria gradually swelled to a larger size structure and finally lost fluorescence. This indicates that mitochondrial membrane potential is lost during the swelling process after compound treatment.

3.6. Molecular cell death mechanisms

Finally, to understand the molecular cell death mechanisms triggered by these compounds, cells were treated with compound **2** and several proteins involved in stress response, autophagy and apoptosis were analysed. Activation of p38 Mitogen-Activated Protein Kinase

(MAPK) in A549 cells was observed in a dose-response manner (Figure 7a). This signal has been reported to activate apoptosis after some stresses. After 24 h of treatment with higher concentrations of compound **2**, we were able to observe a small activation of caspase 9 and 3, as well as PARP cleavage (Figure 7b). Likewise, no statistically significant effects in apoptotic markers were observed after 48 h treatment. To further analyse whether this apoptotic activation was involved in the cytotoxic effect induced by tambjamines, a pan-caspase inhibitor (10 μ M Z-VAD-FMK) was added before treatment with compound **2**. Under these conditions, cell viability was not recovered (data not shown). Therefore, this result suggested that although apoptosis is being triggered by these tambjamine analogues, this process is not entirely responsible for the cytotoxic effect induced by these compounds.

This led us to study the autophagic process after compound treatment and to investigate whether it was involved in the observed cytotoxicity. At very low concentrations of compound **2** (IC_{25}), an impressive appearance of the lipidated LC3 form (LC3-II), indicative of autophagosome formation (Figure 7c), was detected. On the other hand, p62, a protein that is itself degraded by autophagy, was not degraded but accumulated after treatment, indicating a blockade of the autophagic flux. To elucidate whether autophagy was involved in the induced cell death, an inhibitor of autophagosomes formation (5 mM 3-MA) was added prior compound administration (data not shown). Cell viability was not recovered after 3-MA administration, suggesting that autophagosomes formation and their accumulation are not crucial for the cytotoxic effect induced by tambjamines. Finally, at higher doses and 24 h of treatment, tambjamines also provoked cytoplasmic swelling, which finally led to plasma membrane breakdown indicative of necrosis, as observed in the phase contrast images (Figure 3b) and the supplementary video.

4. Discussion

Diverse synthetic tambjamine analogues have recently shown potent anticancer activity in a panel of cancer cell lines, including human melanoma, lung carcinoma, colorectal adenocarcinoma and mammary adenocarcinoma cells [19, 20]. In this study, we extend the results obtained with those compounds bearing 4-alkoxy-2,2'-bipyrrole moieties [19] to several lung cancer cell lines and CSC, as well as characterize in deep for the first time the

cellular and molecular events that are participating in the cell death induced by these potent compounds.

Cell viability was significantly reduced by most of the tested compounds in all human lung cancer cell lines studied, and compound **2** showed to be especially potent against patient-derived CSC. This tumour subpopulation possesses tumour-initiating and self-renewal capacities, and contributes to acquired chemotherapy resistance in cancer [25], thus these results are very promising for lung cancer treatment and the prevention of tumour recurrences. In this view, other anionophores such as the recently reported 2-pyrrolylindole tambjamine analogues or the cation selective ionophore salinomycin, also induce CSC-specific toxicity [20, 26], indicating that the application of these kind of compounds might be a very promising therapy.

Once the cells internalize these synthetic tambjamine analogues, several cellular processes occur, converging in the potent cytotoxic effect observed. On one hand, a huge cytoplasmic vacuolization was detected after compound treatment, which was due to mitochondrial swelling, as demonstrated by several specific markers of this organelle. Moreover, after significant organelle swelling, loss of mitochondrial membrane potential was induced by compound **2**. Mitochondria in eukaryotic cells are the essential machinery to provide energy with an aerobic environment. It has previously been described in cells with acute cellular injury that mitochondrial depolarization and mitochondrial membrane permeabilization lead to a large amplitude swelling and cellular ATP depletion [27, 28]. Therefore, mitochondrial dysfunction observed after tambjamine analogues treatment may cause an energetic failure contributing to their cytotoxic effect.

Autophagy is a catabolic process whereby cellular components are enclosed in double-membrane vesicles referred to as autophagosomes, targeting them for lysosomal degradation. This process serves as an essential cytoprotective response to pathologic stresses [29]. Accumulation of defective mitochondria triggers its selective degradation, process known as mitochondrial autophagy or mitophagy, maintaining a healthy population of these organelles [30, 31]. A very significant amount of the autophagosomal marker LC3II protein accumulates after treatment with tambjamine analogues, even at very low concentrations. This indicates that the process of autophagy is being triggered by the

treatment with these tambjamine analogues and that the induced mitochondrial damage may launch the process of mitophagy in order to remove damaged organelles. This phenomenon is frequently found as a result of mitochondrial stress, such is the case of treatment with the mitochondrial chain uncoupler carbonyl cyanide m-chlorophenylhydrazone (CCCP)[32], or salinomycin, an ionophore which affects mitochondrial potential [33]. On the other hand, it has recently been reported that pH changes modulate both autophagy and mitophagy [34], thus the changes in cellular pH caused by these compounds could also be contributing to trigger this pathway [20].

The loss of the typical acridine orange fluorescence in acidic organelles after exposure to our compounds indicates lysosomal alkalization. This increase in lysosomal pH is consistent with an anion carrier activity across cellular membranes, similarly to that observed in model liposomes. Interestingly, it has recently been reported that obatoclox, other anionophore related to the prodiginine family which has been evaluated in clinical trials for different cancer conditions, rapidly localizes to the lysosomes and also induces lysosomal alkalization [35, 36].

Lysosomes contain many different types of hydrolytic enzymes that usually exert their maximal enzymatic activity at low pH [37]. Typically, an increase in lysosomal pH could derive from H⁺ leakage, a defective proton pump or lysosomal permeabilization [38]. This could lead to a failure in their proper functioning, resulting in blockade of autophagy [39, 40]. After tambjamine analogues treatment, increase in the lysosomal pH derived from lysosomal membrane permeabilization may inactivate its hydrolytic enzymes and therefore it may block autophagy. This feature mainly occurs because this organelle is essential in the final step of the autophagic process, wherein autophagosomes fuse with lysosomes and subsequent protein digestion occurs [41]. The autophagic substrate, p62, also known as sequestosome 1 (SQSTM1), binds ubiquitinated proteins for subsequent degradation in lysosomes, where it is also degraded [42]. Our results show that there is no p62 degradation, indicating an impairment in the autophagic flux and consequent accumulation of unprocessed autophagosomes or autolysosomes [43]. Moreover, the autophagy inhibitor 3-MA, which inhibits autophagy by blocking autophagosomes formation via the inhibition of type III Phosphatidylinositol 3-kinases, is not able to reverse the cytotoxic effect induced by tambjamins. Thus this autophagy might be contributing to the cytotoxic effect, but it is not

responsible for it. Nevertheless, mitochondrial dysfunction along with a defect in autophagy catabolism due to lysosomal deacidification might be detrimental to tumor cells since they produce low rates of ATP and impaired recycling of nutrients for energy production, as well as an imbalance in vesicular biogenesis and turnover. This cellular stress is reflected by p38 MAPK activation, which may initiate apoptosis [44], although again this process is not crucial for the observed cytotoxicity elicited by these compounds. Therefore, the imbalance in cellular ion homeostasis that triggers mitochondrial dysfunction and lysosomal deacidification may be inducing cell death by necrosis after tambjamine analogues treatment. In this regard, the lysosomal permeabilization induced by obatoclax in apoptosis-resistant anaplastic thyroid cells has been demonstrated to be sufficient to induce necrosis in this resistant model, representing an interesting therapeutic approach [36].

Overall, these new tambjamine analogues show promising anticancer properties in lung cancer and could represent a good therapeutic option for apoptosis-resistant tumors. These results shed light into the cellular and molecular mechanisms resulting from the action of these compounds. Lysosomal and mitochondrial dysfunction led to necrosis as the main cell death mechanism responsible for the cytotoxicity of these compounds, which might be shared by other active small molecule anionophores.

Acknowledgements

This work was supported by a grant from the Spanish government and the EU (FIS PI13/00089), a grant from La Marató de TV3 Foundation (20132730), Consejería de Educación de la Junta de Castilla y León (BU340U13 and BU092U16). The authors would like to thank Dr. Jantus-Lewintre and Dr. Calabuig-Fariñas for their assistance with cancer stem cell cultures. Moreover, the authors also thank Benjamín Torrejón from CCiT (Centres Científics i Tecnològics, Campus de Bellvitge, Universitat de Barcelona) for his technical support. E.H. thanks the Junta de Castilla y León (Consejería de Educación) and Fondo Social Europeo for a PIRTU contract.

Conflict of interest

The authors declare no conflict of interest.

References

- [1] C.A. Hübner, T.J. Jentsch, Ion channel diseases, *Human molecular genetics*. 11 (2002) 2435-45.
- [2] A. Becchetti, Ion channels and transporters in cancer. 1. Ion channels and cell proliferation in cancer, *Am J Physiol Cell Physiol*. 301 (2011) C255-65.
- [3] V. Lehen'kyi, G. Shapovalov, R. Skryma, N. Prevarskaya, Ion channels and transporters in cancer. 5. Ion channels in control of cancer and cell apoptosis, *Am J Physiol Cell Physiol*. 301 (2011) C1281-9.
- [4] B.A. Webb, M. Chimenti, M.P. Jacobson, D.L. Barber, Dysregulated pH: a perfect storm for cancer progression, *Nat Rev Cancer*. 11 (2011) 671-7.
- [5] J. Ferlay, I. Soerjomataram, M. Ervik, R. Dikshit, S. Eser, C. Mathers, et al. GLOBOCAN 2012 v1.0, Cancer Incidence and Mortality Worldwide: IARC CancerBase No. 11 [Internet]. Lyon, France: International Agency for Research on Cancer; 2013. Available from: <http://globocan.iarc.fr>, accessed on 25/07/2016.
- [6] S. Cooper, S.G. Spiro, Small cell lung cancer: treatment review, *Respirology*. 11 (2006) 241-8.
- [7] R. Rosell, F. Cecere, M. Santarpia, N. Reguart, M. Taron, Predicting the outcome of chemotherapy for lung cancer, *Current opinion in pharmacology*. 6 (2006) 323-31.
- [8] N. Busschaert, P.A. Gale, Small-Molecule Lipid-Bilayer Anion Transporters for Biological Applications, *Angewandte Chemie International Edition*. 52 (2013) 1374-82.
- [9] P.A. Gale, R. Pérez-Tomás, R. Quesada, Anion transporters and biological systems, *Accounts of chemical research*. 46 (2013) 2801-13.
- [10] E. Llagostera, V. Soto-Cerrato, B. Montaner, R. Perez-Tomas, Prodigiosin induces apoptosis by acting on mitochondria in human lung cancer cells, *Ann N Y Acad Sci*. 1010 (2003) 178-81.
- [11] R. Pérez-Tomás, B. Montaner, E. Llagostera, V. Soto-Cerrato, The prodigiosins, proapoptotic drugs with anticancer properties, *Biochem Pharmacol*. 66 (2003) 1447-52.
- [12] V. Soto-Cerrato, E. Llagostera, B. Montaner, G.L. Scheffer, R. Perez-Tomas, Mitochondria-mediated apoptosis operating irrespective of multidrug resistance in breast cancer cells by the anticancer agent prodigiosin, *Biochem Pharmacol*. 68 (2004) 1345-52.
- [13] N.R. Williamson, P.C. Fineran, T. Gristwood, S.R. Chawrai, F.J. Leeper, G.P. Salmond, Anticancer and immunosuppressive properties of bacterial prodiginines. (2007).
- [14] J.L. Sessler, L.R. Eller, W.S. Cho, S. Nicolaou, A. Aguilar, J.T. Lee, et al., Synthesis, Anion-Binding Properties, and In Vitro Anticancer Activity of Prodigiosin Analogues, *Angewandte Chemie International Edition*. 44 (2005) 5989-92.
- [15] N. Busschaert, C. Caltagirone, W. Van Rossom, P.A. Gale, Applications of supramolecular anion recognition, *Chemical reviews*. 115 (2015) 8038-155.
- [16] M. Carbone, C. Irace, F. Costagliola, F. Castelluccio, G. Villani, G. Calado, et al., A new cytotoxic tambjamine alkaloid from the Azorean nudibranch *Tambja ceutae*, *Bioorganic & medicinal chemistry letters*. 20 (2010) 2668-70.
- [17] B.C. Cavalcanti, H.V. Júnior, M.H. Selegim, R.G. Berlinck, G.M. Cunha, M.O. Moraes, et al., Cytotoxic and genotoxic effects of tambjamine D, an alkaloid isolated from the nudibranch *Tambja eliora*, on Chinese hamster lung fibroblasts, *Chem-Biol Interact*. 174 (2008) 155-62.
- [18] P.I. Hernández, D. Moreno, A.A. Javier, T. Torroba, R. Pérez-Tomás, R. Quesada, Tambjamine alkaloids and related synthetic analogs: efficient transmembrane anion transporters, *Chemical Communications*. 48 (2012) 1556-8.
- [19] E. Hernando, V. Soto-Cerrato, S. Cortes-Arroyo, R. Perez-Tomas, R. Quesada, Transmembrane anion transport and cytotoxicity of synthetic tambjamine analogs, *Org Biomol Chem*. 12 (2014) 1771-8.
- [20] V. Soto-Cerrato, P. Manuel-Manresa, E. Hernando, S. Calabuig-Fariñas, A. Martinez-Romero, V.c. Fernández-Dueñas, et al., Facilitated Anion Transport Induces Hyperpolarization of the Cell Membrane that Triggers Differentiation and Cell Death in Cancer Stem Cells, *J Am Chem Soc*. 137 (2015) 15892-8.
- [21] M.B. Hansen, S.E. Nielsen, K. Berg, Re-examination and further development of a precise and rapid dye method for measuring cell growth/cell kill, *Journal of immunological methods*. 119 (1989) 203-10.

- [22] S.G. Olenych, N.S. Claxton, G.K. Ottenberg, M.W. Davidson, The fluorescent protein color palette, *Curr Protoc Cell Biol.* Chapter 21 (2007) Unit 21 5.
- [23] A. Allison, M. Young, Vital staining and fluorescence microscopy of lysosomes, *Lysosomes in biology and pathology.* 2 (1969) 600-28.
- [24] W. Pendergrass, N. Wolf, M. Poot, Efficacy of MitoTracker Green™ and CMXRosamine to measure changes in mitochondrial membrane potentials in living cells and tissues, *Cytometry Part A.* 61 (2004) 162-9.
- [25] P. Valent, D. Bonnet, R. De Maria, T. Lapidot, M. Copland, J.V. Melo, et al., Cancer stem cell definitions and terminology: the devil is in the details, *Nature Reviews Cancer.* 12 (2012) 767-75.
- [26] P.B. Gupta, T.T. Onder, G. Jiang, K. Tao, C. Kuperwasser, R.A. Weinberg, et al., Identification of selective inhibitors of cancer stem cells by high-throughput screening, *Cell.* 138 (2009) 645-59.
- [27] J.J. Lemasters, A.-L. Nieminen, T. Qian, L.C. Trost, S.P. Elmore, Y. Nishimura, et al., The mitochondrial permeability transition in cell death: a common mechanism in necrosis, apoptosis and autophagy, *Biochimica et Biophysica Acta (BBA)-Bioenergetics.* 1366 (1998) 177-96.
- [28] J.-S. Kim, L. He, J.J. Lemasters, Mitochondrial permeability transition: a common pathway to necrosis and apoptosis, *Biochem Biophys Res Commun.* 304 (2003) 463-70.
- [29] L. Murrow, J. Debnath, Autophagy as a stress response and quality control mechanism—implications for cell injury and human disease, *Annual review of pathology.* 8 (2013) 105.
- [30] D.A. Kubli, Å.B. Gustafsson, Mitochondria and mitophagy the yin and yang of cell death control, *Circulation research.* 111 (2012) 1208-21.
- [31] I. Kim, S. Rodriguez-Enriquez, J.J. Lemasters, Selective degradation of mitochondria by mitophagy, *Arch Biochem Biophys.* 462 (2007) 245-53.
- [32] K.-Y. Kwon, B. Viollet, O.J. Yoo, CCCP induces autophagy in an AMPK-independent manner, *Biochem Biophys Res Commun.* 416 (2011) 343-8.
- [33] J.R. Jangamreddy, S. Ghavami, J. Grabarek, G. Kratz, E. Wiechec, B.-A. Fredriksson, et al., Salinomycin induces activation of autophagy, mitophagy and affects mitochondrial polarity: differences between primary and cancer cells, *Biochimica et Biophysica Acta (BBA)-Molecular Cell Research.* 1833 (2013) 2057-69.
- [34] A.V. Berezhnov, M.P. Soutar, E.I. Fedotova, M.S. Frolova, H. Plun-Favreau, V.P. Zinchenko, et al., Intracellular pH modulates autophagy and mitophagy, *J Biol Chem.* (2016) jbc. M115. 691774.
- [35] V.A. Stamelos, N. Fisher, H. Bamrah, C. Voisey, J.C. Price, W.E. Farrell, et al., The BH3 Mimetic Obatoclox Accumulates in Lysosomes and Causes Their Alkalinization, *PLoS ONE.* 11 (2016) e0150696.
- [36] D. Champa, A. Orlicchio, B. Patel, M. Ranieri, A.A. Shemetov, V.V. Verkhusa, et al., Obatoclox kills anaplastic thyroid cancer cells by inducing lysosome neutralization and necrosis, *Oncotarget.* 5 (2016).
- [37] J. Coffey, C. de Duve, Digestive activity of lysosomes I. The digestion of proteins by extracts of rat liver lysosomes, *J Biol Chem.* 243 (1968) 3255-63.
- [38] P. Boya, Lysosomal function and dysfunction: mechanism and disease, *Antioxidants & redox signaling.* 17 (2012) 766-74.
- [39] B. Levine, G. Kroemer, Autophagy in the pathogenesis of disease, *Cell.* 132 (2008) 27-42.
- [40] M. Merschtik, K.M. Ryan, Lysosomal proteins in cell death and autophagy, *FEBS journal.* 282 (2015) 1858-70.
- [41] G. Kroemer, M. Jäätelä, Lysosomes and autophagy in cell death control, *Nature Reviews Cancer.* 5 (2005) 886-97.
- [42] G. Bjørkøy, T. Lamark, S. Pankiv, A. Øvervatn, A. Brech, T. Johansen, Monitoring autophagic degradation of p62/SQSTM1, *Methods Enzymol.* 452 (2009) 181-97.
- [43] M. Komatsu, Y. Ichimura, Physiological significance of selective degradation of p62 by autophagy, *FEBS letters.* 584 (2010) 1374-8.
- [44] T. Wada, J.M. Penninger, Mitogen-activated protein kinases in apoptosis regulation, *Oncogene.* 23 (2004) 2838-49.

Figure Legends

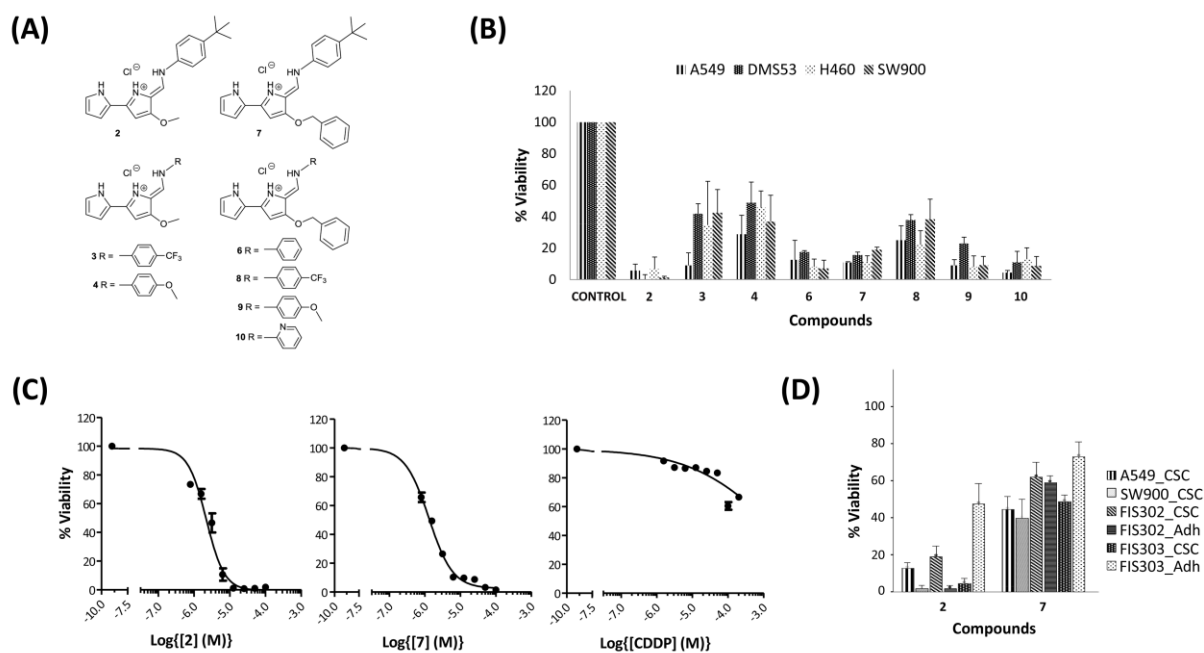


Figure 1. Synthetic tambjamine analogues significantly decrease cell viability. (A) Chemical structure of synthetic tambjamine analogues. **(B)** MTT cell viability assay was performed after 24 h of treatment with synthetic tambjamine analogues at 10 μ M in A549, DMS53, H460 and SW900 cell lines. **(C)** Concentrations ranging from 0.8 to 100 μ M of compounds **2** and **7** were used in dose-response curve experiments for IC₅₀ value calculation in A549 cell line, at the same time, in case of positive control, concentrations ranging from 1.6 to 200 μ M of cisplatin (CDDP) were tested. **(D)** Cell viability was tested in adherent (Adh) and cancer stem cells (CSC) derived from lung cancer patients or cancer cell lines after 10 μ M of compound **2** for 24 h. Results show the mean value \pm SD of at least three independent experiments.

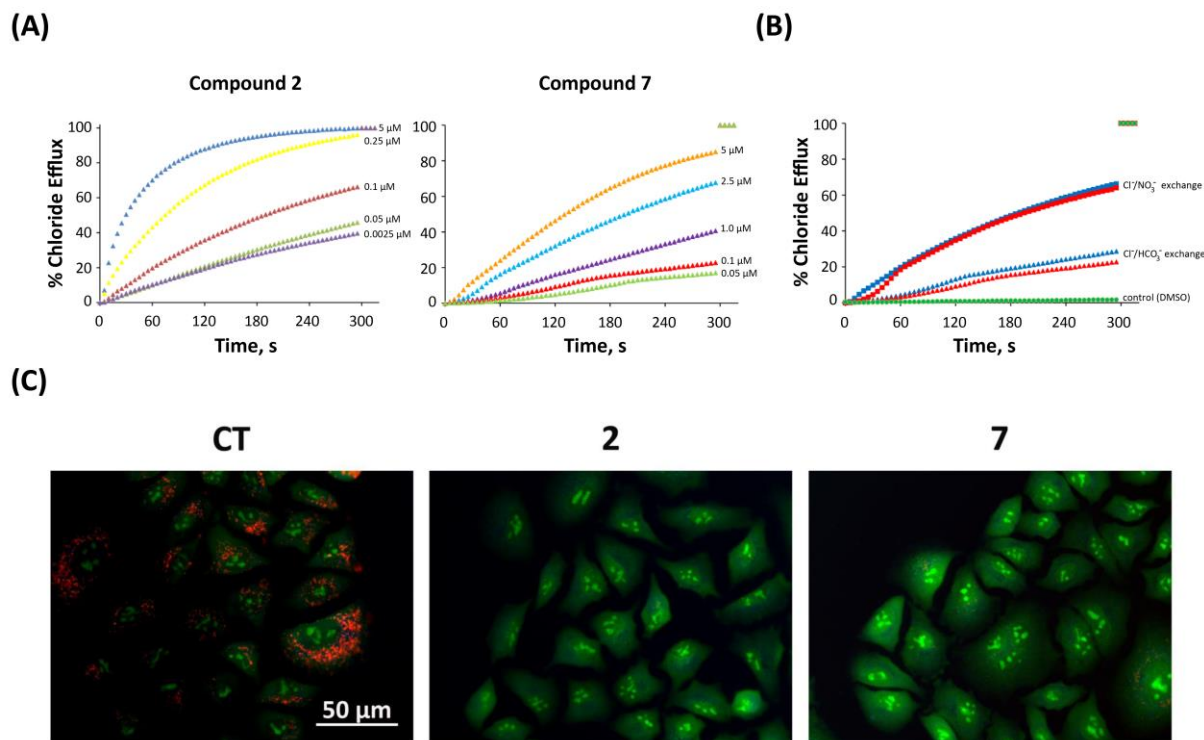


Figure 2. Potent transmembrane anion transport activity of tambjamine analogues in liposomes and cellular models. (A) Chloride efflux upon addition of compound **2** or **7** at different concentrations to vesicles composed of POPC. **(B)** Impact of external buffer (NaNO_3 , squared symbols, or $\text{NaHCO}_3/\text{Na}_2\text{SO}_4$, triangular symbols) in the chloride efflux promoted by **2** or **7** ($0.1 \mu\text{M}$, blue and red symbols, respectively) (See section 2.2. for details). Each trace represents an average of at least three different experiments. **(C)** Acridine orange staining on A549 cells treated with vehicle (DMSO), $10 \mu\text{M}$ compound **2** or **7** for 1 h. Images are representative of three independent experiments.

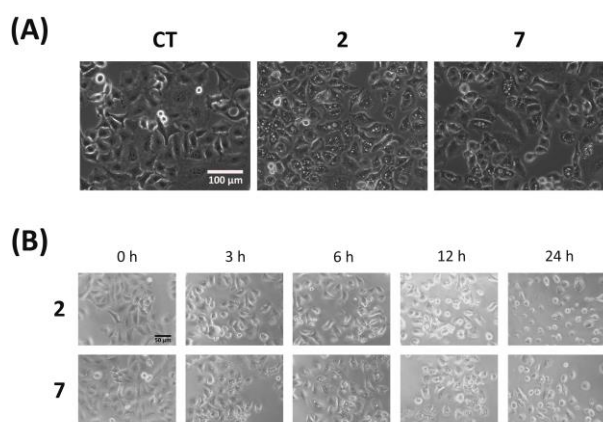


Figure 3. Cytoplasmic vacuolization induced by tambjamine analogues. (A) Phase contrast microscopy images of A549 cells treated with IC_{75} of compounds **2** or **7** for 6 h. **(B)** Time-course photographs of A549 cells treated with $10 \mu\text{M}$ compounds **2** or **7** for 0 h, 3 h, 6 h, 12 h, and 24 h.

μM of compound **2** or **7** during 24 h. Scale bars 100 μm (**A**) and 50 μm (**B**). Images are representative of three independent experiments.

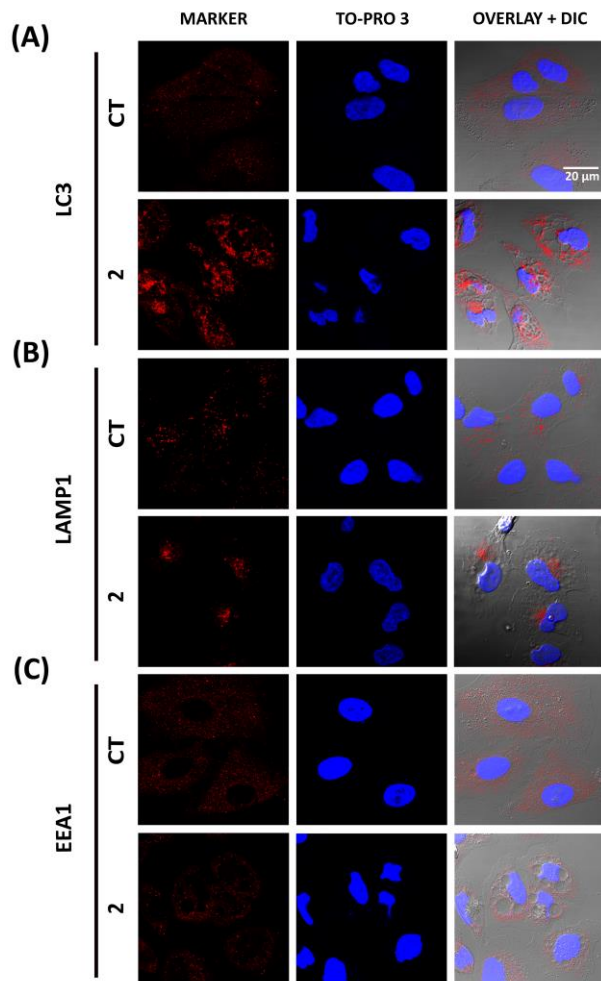


Figure 4. Tambjamine analogues treatment

did not induce swelling of autophagosomes, lysosomes or early endosomes. Immunofluorescence in A549 cells treated with IC_{75} of compound **2** for 6 h. It was performed with different antibodies that recognize several cellular organelles (red) and were compared to the distribution of cytoplasmic vacuoles observed by phase contrast microscopy. **(A)** Distribution of the autophagosomal marker LC3, **(B)** distribution of lysosomal marker LAMP1 **(C)** distribution of the early endosome marker EEA1. The nucleus was counterstained with TOPRO-3 (blue). Scale bar 20 μm . Images are representative of at least three independent experiments.

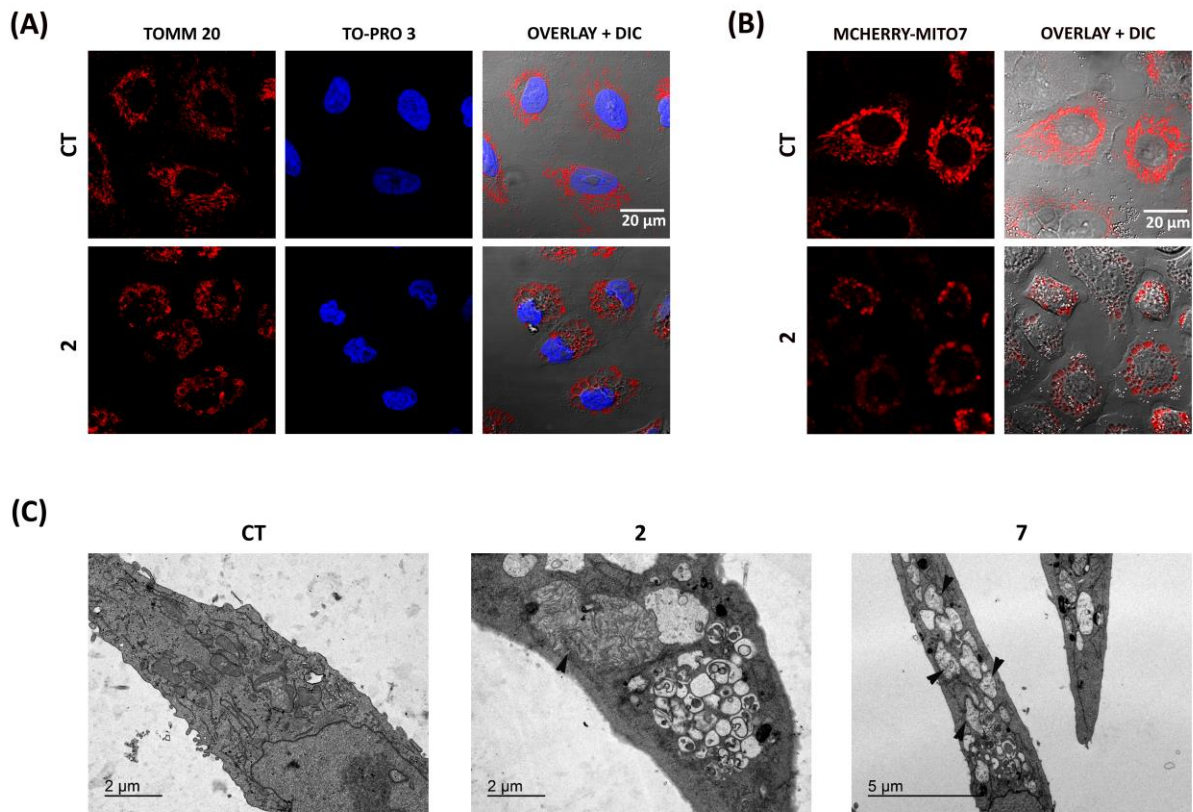


Figure 5. Mitochondrial swelling after tambjamine analogues treatment. (A) Immunofluorescence of mitochondrial marker TOMM20 in A549 cells treated with IC₇₅ of compound **2** for 6 h. The nucleus was counterstained with TOPRO-3 (blue). **(B)** A549 cells overexpressing mCherry-Mito7 plasmid, which targets mitochondria (red), were treated with IC₇₅ of compound **2** for 3 h. Mitochondrial staining was compared to vacuolization observed in phase contrast photographs. Scale bar 20 μm . **(C)** Transmission electron micrographs from control and treated A549 cells with compound **2** and **7** for 6 h. Mitochondrial swelling (black arrows) as well as double-membrane vesicles accumulation (autophagosomes and autolysosomes) were observed. Scale bar 2 and 5 μm . Images are representative of at least three independent experiments.

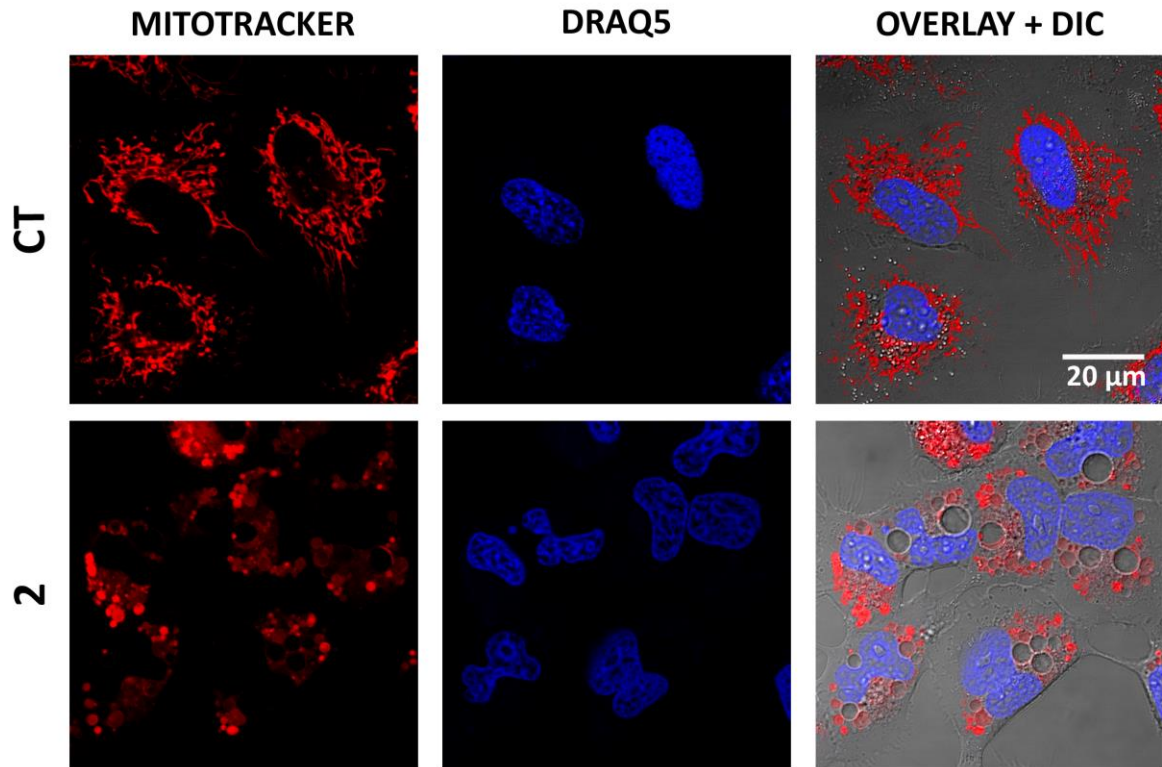


Figure 6. Mitochondrial swelling and loss of mitochondrial membrane potential after tambjamine analogues treatment. Confocal images of A549 cells treated with 500 nM MitoTracker Red CMXRos during 1 h and then compound **2** for 3 h. Mitochondria with normal membrane potential are stained in red. Nucleus was counterstained with DRAQ5 (blue). Scale bar 20 μm . Images are representative of at least three independent experiments.

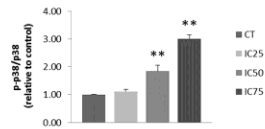
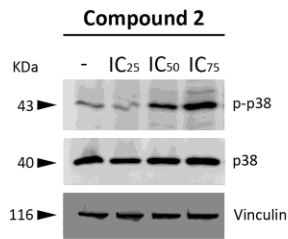
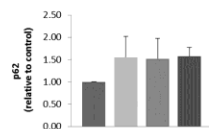
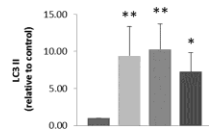
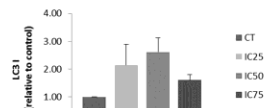
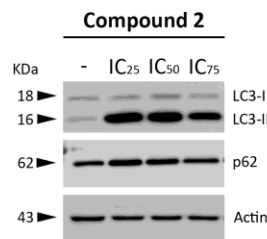
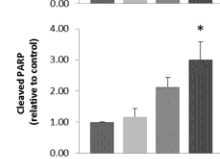
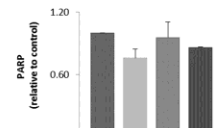
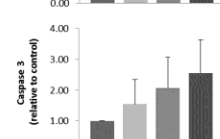
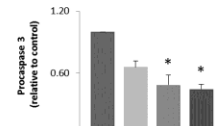
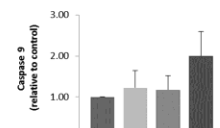
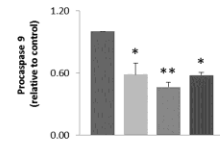
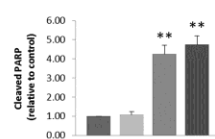
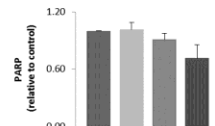
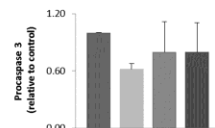
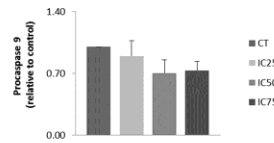
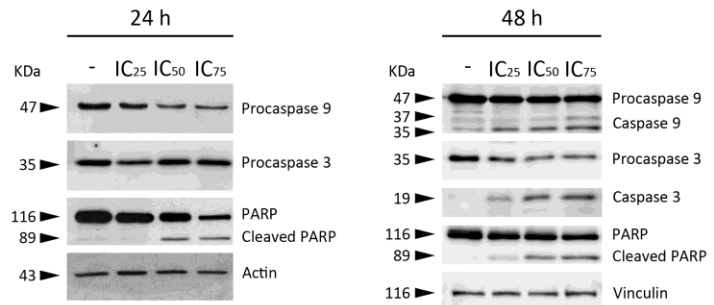
(A)**(C)****(B)****Compound 2**

Figure 7. p38 MAPK activation, apoptosis induction and autophagy blockade after tambjamine analogues treatment. A549 cells were treated with compound **2** IC₂₅, IC₅₀ and IC₇₅ values for 24 h and protein extracts were used to determine changes in protein levels. Detection and quantification of: **(A)** the stress kinase p38 MAPK and its phosphorylation levels; **(B)** apoptotic markers such as caspase 9, 3 and PARP substrate and **(C)** autophagic markers like LC3II and p62. Protein levels were normalized with their respective loading controls (actin or vinculin) in each blot. Fold changes in protein expression levels were quantified and referred to non-treated cells. Data show the mean \pm SEM of three

independent experiments. Statistically significant results are indicated as * $p < 0.05$ and ** $p < 0.01$.

Supplementary video legend.

Cellular swelling and plasmatic membrane breakdown indicative of necrosis after tambjamine analogues treatment. A549 cells (1×10^4 cells/well) were seeded in 8-well sterile μ -Slide chambered coverslip (Ibidi) and allowed to attach and grow during 72 h. Then cells were treated with IC_{75} of compound **2** and recorded during 6 h.